Title

Mechanochemotransduction During Cardiomyocyte Contraction Is Mediated by Localized Nitric Oxide Signaling

Journal

Science Signaling, 7(317)

ISSN

1945-0877

Authors

Jian, Zhong

Han, Huilan

Zhang, Tieqiao

et al.

Publication Date

2014-03-18

DOI

10.1126/scisignal.2005046

Peer reviewed

Published in final edited form as:
Sci Signal. ; 7(317): ra27. doi:10.1126/scisignal.2005046.

Mechanochemotransduction During Cardiomyocyte Contraction Is Mediated by Localized Nitric Oxide Signaling

Zhong Jian[1,*], **Huilan Han**[1,*], **Tieqiao Zhang**[2,*], **Jose Puglisi**[1], **Leighton T. Izu**[1], **John A. Shaw**[3], **Ekama Onofiok**[4], **Jeffery R. Erickson**[1], **Yi-Je Chen**[1], **Balazs Horvath**[1,5], **Rafael Shimkunas**[1,6,7], **Wenwu Xiao**[4], **Yuanpei Li**[4], **Tingrui Pan**[6], **James Chan**[2], **Tamas Banyasz**[1,5], **Jil C. Tardiff**[8], **Nipavan Chiamvimonvat**[7], **Donald M. Bers**[1], **Kit S. Lam**[4], and **Ye Chen-Izu**[1,6,7,†]

[1]Department of Pharmacology, University of California, Davis, Davis, CA 95616, USA

[2]Center for Biophotonics Science and Technology, University of California, Davis, Davis, CA 95616, USA

[3]Department of Aerospace Engineering, University of Michigan, Ann Arbor, MI 48109, USA

[4]Department of Biochemistry and Molecular Medicine, University of California, Davis, Davis, CA 95616, USA

[5]Department of Physiology, University of Debrecen, Medical and Health Science Centre, 4012 Debrecen, Hungary

[6]Department of Biomedical Engineering, University of California, Davis, Davis, CA 95616, USA

[7]Department of Internal Medicine (Cardiology), University of California, Davis, Davis, CA 95616, USA

[8]Department of Medicine, University of Arizona, Tucson, AZ 85721, USA

Abstract

Cardiomyocytes contract against a mechanical load during each heartbeat, and excessive mechanical stress leads to heart diseases. Using a cell-in-gel system that imposes an afterload during cardiomyocyte contraction, we found that nitric oxide synthase (NOS) was involved in transducing mechanical load to alter Ca^{2+} dynamics. In mouse ventricular myocytes, afterload increased the systolic Ca^{2+} transient, which enhanced contractility to counter mechanical load, but also caused spontaneous Ca^{2+} sparks during diastole that could be arrhythmogenic. The increases in the Ca^{2+} transient and sparks were attributable to increased ryanodine receptor (RyR) sensitivity because the amount of $Ca2^{+}$ in the sarcoplasmic reticulum load was unchanged. Either

†Corresponding author: ychenizu@ucdavis.edu.
*These authors contributed equally to this work.

Supplementary Materials: www.sciencesignaling.org/cgi/content/full/7/317/ra27/DC1

Author contributions: Project and experimental designs were done by Y.C.-I., K.S.L., L.T.I., J.C.T., T.B., N.C., and D.M.B. Chemical synthesis and purification were done by E.O., W.X., Y.L., and K.S.L. Transgenic mouse R92Q was provided by J.C.T. Experiments were performed by Z.J., H.H., T.Z., J.R.E., Y.-J.C., B.H., R.S., and Y.C.-I. Data analyses and statistical tests were performed by Z.J., H.H., T.Z., J.P., L.T.I., J.A.S., J.R.E., R.S., T.P., J.C., and Y.C.-I. Manuscript writing and editing were done by Y.C.-I., H.H., L.T.I., N.C., K.S.L., and D.M.B.

Competing interests: The authors declare that they have no competing interests.

pharmacological inhibition or genetic deletion of nNOS (or NOS1), but not of eNOS (or NOS3), prevented afterload-induced $Ca2^+$ sparks. This differential effect may arise from localized NO signaling, arising from the proximity of nNOS to RyR, as determined by super-resolution imaging. Ca^{2+}-calmodulin–dependent protein kinase II (CaMKII) and nicotinamide adenine dinucleotide phosphate oxidase 2 (NOX2) also contributed to afterload-induced Ca^{2+} sparks. Cardiomyocytes from a mouse model of familial hypertrophic cardiomyopathy exhibited enhanced mechanotransduction and frequent arrhythmogenic Ca^{2+} sparks. Inhibiting nNOS and CaMKII, but not NOX2, in cardiomyocytes from this model eliminated the $Ca2^+$ sparks, suggesting mechanotransduction activated nNOS and CaMKII independently from NOX2. Thus, our data identify nNOS, CaMKII, and NOX2 as key mediators in mechanochemotransduction during cardiac contraction, which provides new therapeutic targets for treating mechanical stress–induced Ca^{2+} dysregulation, arrhythmias, and cardiomyopathy.

Introduction

The heart must pump blood against mechanical loads that constantly change with physical activity, posture, emotion, and pathophysiological states. The Anrep effect (1–4) describes an enhancement of cardiac contractility resulting from increased afterload, which is complementary to the Frank-Starling mechanism that describes enhanced contractility from increased preload (5). Petroff *et al.* (6) have found that stretching cardiomyocytes to increase preload can induce spontaneous Ca^{2+} sparks by activating the nitric oxide synthase 3 (or eNOS). Prosser *et al.* (7, 8) have shown that stretching cardiomyocytes activates nicotinamide adenine dinucleotide phosphate oxidase 2 (NOX2) to cause Ca^{2+} sparks. Preload-induced changes in Ca^{2+} handling contribute to the Frank-Starling mechanism. However, it has been incompletely understood whether afterload might also cause changes in Ca^{2+} handling and whether analogous mechanochemotransduction mechanisms could be activated in cardiomyocytes contracting against a mechanical load. Such knowledge is critical for understanding why excessive afterload under pathological conditions such as hypertension, infarction, and asynchronous contraction can lead to cardiac remodeling, hypertrophy, arrhythmias, and heart failure (9–11). Here, we identified nitric oxide synthase 1 (or nNOS), Ca^{2+} -calmodulin-dependent protein kinase II (CaMKII), and NOX2 as key mediators of mechanochemotransduction pathways that transduce mechanical afterload to Ca^{2+} handling. These findings provide new mechanistic understanding of the Anrep effect and help to identify possible molecular targets for treating heart diseases that are induced by mechanical stress.

Results

The cell-in-gel system to impose mechanical load during single cardiomyocyte contraction

Previously investigations of mechanochemotransduction mechanisms have been limited by difficulties in controlling the mechanical load on cardiomyocyte contraction at the single-cell level. We developed a “cell-in-gel” system by embedding freshly isolated cardiomyocytes in a three-dimensional (3D) elastic matrix made of polyvinyl alcohol (PVA) hydrogel and boronic acid cross-linker; the boronate group also cross-linked the cell surface glycans, thereby tethering the cell surface to the gel (Fig. 1A and fig. S1) (12). This system

has several advantages. When the in-gel cardiomyocyte contracts against the gel matrix, the elastic matrix resists the shortening and broadening of the cell during contraction, thereby exerting multiaxial mechanical stress on the cell (Fig. 1B). Furthermore, the stiffness of the gel is tunable by the mixing ratio of the cross-linker and the PVA (13). In addition, the gel matrix is porous to allow rapid bath solution exchange for studying drug effects and is optically transparent for real-time imaging of cell contraction and fluorescence imaging of Ca^{2+} signals. The gel components are nontoxic and do not affect the cell function (fig. S2). This cell-in-gel system mimics the in vivo mechanical environment in two aspects: the imposition of multiaxial 3D mechanical stress during contraction, and the tethering of the cell surface to the gel to impose both normal and shear stresses to the cell surface (14).

Afterload-induced changes in Ca^{2+} handling during systole and diastole

We studied the effects of mechanical stress during cardiomyocyte contraction under mechanical afterload using the cell-in-gel system. The cardiomyocyte was paced at 0.5 Hz to reach steady-state contraction (movie S1) while being continuously perfused with Tyrode solution. Compared to load-free contractions (Fig. 1C), the cardiomyocyte contracting in-gel (Fig. 1D) displayed less fractional shortening (Fig. 1E); it also showed augmented Ca^{2+} transient in systole (Fig. 1F), as well as spontaneous Ca^{2+} sparks during diastole (Fig. 1G). The Ca^{2+} spark rate (sparks per unit area) was low under load-free condition, slightly increased in soft gel (Gel 5%), and significantly increased in stiffer gel (Gel 7.5%). Decoupling contraction from Ca^{2+} signaling using the myosin II inhibitor blebbistatin reduced the Ca^{2+} spark rate to that of the load-free condition (Fig. 1G). These data demonstrate a positive correlation between the mechanical load and the spontaneous Ca^{2+} spark rate. We also examined the systolic Ca^{2+} transient and cardiomyocyte contraction under the above conditions of varying loads. Compared to load-free contraction, cardiomyocyte contraction in soft gel (Gel 5%) under moderate mechanical load did not significantly alter the Ca^{2+} transient; however, cardiomyocyte contraction in stiffer gel (Gel 7.5%) under higher mechanical load significantly increased the Ca^{2+} transient (fig. S3A), although the contraction amplitude decreased due to the higher load (fig. S3B). Blebbistatin treatment attenuated mechanochemotransduction and restored the Ca^{2+} transient to the load-free condition (fig. S3A). Therefore, afterload on cardiomyocytes during contraction increases the systolic Ca^{2+} transient, which enhances contractility to counter mechanical load, but also leads to spontaneous Ca^{2+} sparks during diastole, which are proarrhythmic. In the experiments below, we used the cell-in-gel system with Gel 7.5% to impose mechanical afterload during cardiomyocyte contraction.

Diastolic Ca^{2+} sparks were few during the initial several beats of contraction, but then increased in frequency during subsequent beats (Fig. 2, A and B). Upon cessation of pacing, the sparks disappeared almost immediately. The initial latency suggested a buildup process for mechanochemotransduction to activate the signaling pathways that lead to modulation of ryanodine receptor (RyR) activity and increase of Ca^{2+} sparks. Such latency agrees with a slow onset of the Anrep effect, which takes minutes to develop at the tissue level (3). The disappearance of Ca^{2+} sparks after cessation of pacing is also consistent with a reversible effect of NO signaling (15, 16).

To test whether the increase of Ca^{2+} transient and Ca^{2+} spark rate could be due to increased sarcoplasmic reticulum (SR) Ca^{2+} content, we measured the cytosolic Ca^{2+} concentration and SR content using a Fura-2 ratiometric method. The cardiomyocyte was paced at 0.5 Hz; after reaching steady state, pacing was stopped and caffeine (20 mM) was applied to rapidly release the SR Ca^{2+} content (Fig. 2C). Although the systolic Ca^{2+} transient was increased in the in-gel contracting cardiomyocytes compared to the load-free cardiomyocytes (Fig. 2D), the SR Ca^{2+} content did not show detectable changes (Fig. 2E). Thus, the fractional SR Ca^{2+} release was higher for the cardiomyocytes contracting in-gel, suggesting an increase in RyR sensitivity. Increased RyR sensitivity could also explain the increase of diastolic Ca^{2+} sparks. High RyR sensitivity and diastolic SR Ca^{2+} leak would reduce SR Ca^{2+} content (17), unless it was compensated for by enhanced SR Ca^{2+} uptake through the SR Ca^{2+} adenosine triphosphatase (ATPase) (SERCA) or reduced Ca^{2+} efflux through the Na^{+}/Ca^{2+} exchanger. Indeed, the decline in systolic Ca^{2+} transient was unaltered (Fig. 2F and fig. S4B), indicating that SR Ca^{2+} uptake can reduce the intracellular Ca^{2+} concentration despite greater release. Moreover, in-gel cardiomyocytes showed a slower decline of the caffeine-induced Ca^{2+} transient (Fig. 2G), indicating that the Ca^{2+} efflux through the Na^{+}/Ca^{2+} exchanger and the sarcolemma Ca^{2+} pump was reduced. These changes allow cardiomyocytes to maintain normal SR Ca^{2+} content despite increased SR Ca^{2+} release.

Localized nNOS and eNOS signaling in mechanochemotransduction

We next examined whether nitric oxide signaling played a role in mediating afterload-induced changes in Ca^{2+} handling. Cardiomyocytes were paced at 0.5 Hz until contraction reached steady state. In-gel cardiomyocytes displayed a high spontaneous Ca^{2+} spark rate (Fig. 3, A and B). The general NOS inhibitor L-NAME (N^{G}-nitro-L-arginine methyl ester) effectively suppressed Ca^{2+} sparks (Fig. 3B), indicating that NOS signaling is essential for mechanochemotransduction. Next, we assessed the contributions of the neuronal isoform (nNOS or NOS1) and the endothelial isoform (eNOS or NOS3) of NOS, both of which are constitutively expressed ventricular myocytes (18). Ca^{2+} sparks were not suppressed by inhibition of eNOS with L-Nio-dihydrochloride (L-Nio) (Fig. 3, A and B), but were suppressed by inhibition of nNOS using N^{ω}-propyl-L-arginine hydrochloride (L-NPA) (Fig. 3, A and B). These data suggest that nNOS, but not eNOS, mediates afterload-induced spontaneous Ca^{2+} sparks. Furthermore, inhibition of nNOS with L-NPA did not affect the Ca^{2+} transient (fig. S4A), whereas inhibition of eNOS with L-Nio not only reduced the peak Ca^{2+} transient (fig. S4A) but also slowed the rate of the Ca^{2+} transient decline (fig. S4B). These data suggest differential effects of nNOS and eNOS in modulating different Ca^{2+} handling pathways.

Inhibition of nNOS and eNOS also reduced cardiomyocyte contraction (fig. S4C), in accordance to their effects on reducing the Ca^{2+} transient. Interpretation of the contraction data needs to take into account the following complexity. When the cardiomyocyte is pulling mechanical load, the contraction amplitude is expected to decrease. However, without the mechanochemotransductionmediated increase of Ca^{2+} transient, the decrease in contraction would be more pronounced. That is, if the cardiomyocyte was purely elastic, the contraction would be less than that measured in a live cardiomyocyte with active mechanochemotransduction regulation to increase the Ca^{2+} transient. To address this issue,

we have performed mechanical analysis assuming a purely elastic cell without mechanochemotransduction (14). The knockdown factor, or the ratio of the cardiomyocyte shortening in-gel to that in load-free condition, is calculated to have a basal value of 0.2 for the elastic cell (14). However, the experimentally measured knockdown factor was 0.4 for the cardiomyocytes (fig. S4C); hence, the mechanochemotransductionmediated increase in Ca^{2+} transient enhanced contractility. Inhibiting nNOS or eNOS disrupts mechanochemotransduction signaling and, thus, reduced knockdown factor toward the basal value (fig. S4C).

To rule out possible nonspecific effects of pharmacological inhibitors, we also conducted experiments using cardiomyocytes from *nNOS*$^{-/-}$ and *eNOS*$^{-/-}$ mice. The *nNOS*$^{-/-}$ cardiomyocytes showed few afterload-induced Ca^{2+} sparks (Fig. 3, A and C). In contrast, *eNOS*$^{-/-}$ cardiomyocytes exhibited a high Ca^{2+} spark rate during contraction in-gel (Fig. 3, A and D), which was suppressed by inhibiting nNOS (Fig. 3, A and D). Therefore, nNOS, not eNOS, mediates the afterload-induced spontaneous Ca^{2+} sparks.

Because NO is a short-lived local signaling molecule, the selective effect of nNOS compared to eNOS on Ca^{2+} sparks could be explained if nNOS is physically closer than eNOS to RyR. In cardiomyocytes, eNOS has been localized to caveolae (19), and nNOS has been localized at the SR (20) and also sarcolemma (21). For example, nNOS associates with various molecules at different subcellular locales, including SERCA in the SR membrane (22), the plasma membrane Ca^{2+} ATPase (PMCA) in caveolae (20), and the structural protein dystrophin near the sarcolemma and t-tubules (23). The intermolecular distance of RyR to nNOS or eNOS had not been measured. Because confocal resolution cannot resolve these distances (fig. S5), we used super-resolution structured illumination microscopy (SIM) to quantify the colocalization of RyR with nNOS and eNOS. SIM images showed that nNOS was closely colocalized with RyR (Fig. 3E and movie S2), whereas eNOS was located farther from RyR (Fig. 3F and movie S3). Colocalization analyses yielded an overlap coefficient of 0.438 for nNOS-RyR and 0.125 for eNOS-RyR (Fig. 3G). The nearest-neighbor distance histogram (Fig. 3G) also showed significantly different patterns, with nNOS-RyR distance peaking at 0.19 μm and eNOS-RyR distance at 0.37 μm, a twofold increase. The effective NO signaling range is expected to be influenced by the distance of diffusion, the amount of NO produced by NOS, the buffering capacity, the degradation and removal, and the target modification kinetics. The twofold increase in signaling distance would translate to fourfold slower diffusion time and eightfold reduction in NO concentration at the target site. Together, the above data suggest that the effective range of intracrine NO signaling in cardiomyocytes could be highly localized to within submicrometer distances.

Mechanochemotransduction in cardiomyocytes from a cardiomyopathy model

To further explore the relationship between mechanical stress and Ca^{2+} dynamics, we investigated cardiomyocytes from a mouse model of familial hypertrophic cardiomyopathy with R92Q mutation in cardiac troponin T. The R92Q mutation in human or mouse hearts causes increased myofilament Ca^{2+} sensitivity and is associated with arrhythmias and sudden cardiac death (24–28). An unresolved question is how mutations in contractile

proteins lead to arrhythmias (29, 30). We found that the afterload-induced spontaneous Ca^{2+} spark rate was significantly higher in R92Q cardiomyocytes (Fig. 4, A and B) than in wild-type cardiomyocytes (Fig. 4B). Consistently, the sparks were suppressed by inhibiting nNOS, but not eNOS (Fig. 4, A and B). Our data suggest that increased sensitivity in mechanochemotransduction leads to increased spontaneous Ca^{2+} spark rate, and thus provide a possible explanation for Ca^{2+}-induced arrhythmogenesis in hearts from individuals with familial hypertrophic cardiomyopathy caused by the R92Q mutation (31–34).

Role of NOX2 and CaMKII in afterload-induced mechanochemotransduction

We further tested whether NOX2-ROS signaling, which is activated by preload (8), might also be engaged by afterload. Inhibition of NOX2 using a specific peptide inhibitor gp91ds-tat decreased afterload-induced Ca^{2+} sparks in wild-type, but not in R92Q, cardiomyocytes (Fig. 4B), suggesting that mechanochemotransduction differentially activated NOX2 and nNOS pathways in different models. Because NOX2 can be activated by nNOS signaling (35), a complex interplay between the two is expected, a result that warrants further investigation.

Because CaMKII can phosphorylate RyR to stimulate Ca^{2+} sparks (36), we investigated the effect of CaMKII inhibition and found that the CaMKII blocker KN93 prevented the afterload-induced Ca^{2+} sparks in cardiomyocytes from both wild-type and R92Q mice (Fig. 4B). To further investigate whether NO can activate CaMKII, we used the fluorescence resonance energy transfer (FRET)–based biosensor Camui (37) to measure the CaMKII activation induced by the NO donor SNAP. In human embryonic kidney cells expressing Camui, treatment with high, but not low, concentrations of SNAP increased CaMKII activation (as indicated by reduced FRET) in the presence of EGTA (fig. S6). CaMKII is autonomously activated by phosphorylation of Thr^{286} (38) and by oxidation of Cys^{280}/Met^{281} (39). To test whether one or both of these mechanisms were responsible for SNAP-induced activation of CaMKII, we assessed the effect of SNAP on mutant versions of Camui lacking either the phosphorylation (Thr^{286}) or oxidation (Cys^{280}/Met^{281}) target sites. In both cases, SNAP-dependent activation of CaMKII was preserved (fig. S6). These data indicate that CaMKII is subject to NO-induced activation that is independent of previously described phosphorylation and oxidation pathways.

Discussion

Using a cell-in-gel system, we have identified key molecules involved in mechanochemotransduction that respond to the mechanical load during cardiomyocyte contraction to regulate Ca^{2+} handling. The systolic Ca^{2+} transient is increased by afterload, which contributes to the Anrep effect (3, 4, 40, 41). Both NOS isoforms were involved in increasing the Ca^{2+} transient; however, the afterload-induced spontaneous Ca^{2+} sparks were mediated by nNOS, but not eNOS. The divergent effects of nNOS and eNOS on modulating RyR might be explained by highly localized NO signaling; super-resolution imaging data suggested that the intracrine NO signaling was within submicrometer range in the cardiomyocytes. Our working hypothesis is that nNOS might predominantly modulate RyR

and SERCA because of its closer proximity to the SR, whereas eNOS might predominantly affect the Ca^{2+} handling proteins near the sarcolemma including Na^{+}/Ca^{2+} exchange, sarcolemma Ca^{2+} pump, and L-type Ca^{2+} channels. In addition to NOS, CaMKII and NOX2 were also involved in afterload-associated mechanochemotransduction during cardiomyocyte contraction. Furthermore, we found that selective inhibition of nNOS and CaMKII suppressed afterload-induced spontaneous Ca^{2+} activities in a model of familial hypertrophic cardiomyopathy, which is associated with a high incidence of cardiac arrhythmias (28, 42, 43). Hence, the mechano–NOS-CaMKII pathways we described here provide a working model (Fig. 4C) that, in combination with other pathways involving NOX (8), angiotensin II (44), transient receptor potential canonical channels (45), and others [review by (4)], help in understanding the mechanical stress effects on the heart. Mechanochemotransduction through NOS and CaMKII signaling pathways suggests novel points of therapeutic intervention for treating mechanical stress–induced Ca^{2+} dysregulation, arrhythmias, and cardiomyopathy.

Materials and Methods

All laboratory procedures conform to the *Guide for the Care and Use of Laboratory Animals* published by the U.S. National Institutes of Health. Animal usage was approved by the local Institutional Animal Care and Use Committee.

Cell isolation

Wild-type and transgenic mice were purchased from The Jackson Laboratory: C57BL/6J (wild type), B6.129S4-Nos1tm1Plh/J (*NOS1*$^{-/-}$), and B6.129P2-Nos3tm1Unc/J (*NOS3*$^{-/-}$). Transgenic mouse with R92Q mutation in cardiac troponin T was created in Tardiff's laboratory (25) and bred in Chen-Izu's laboratory. All mice used in the experiments were 12 to 18 weeks old and male. A standard enzymatic technique (46) was used to isolate the ventricular myocytes using Worthington collagenase type II and Sigma protease type XIV. All experiments were conducted at 21° to 22°C.

Cell-in-gel system

Elastic gel matrix was made of a PVA hydrogel system composed of underivatized PVA (98 kD) and a tetravalent boronate-PEG cross-linker (12). Freshly isolated cardiomyocytes were first suspended in 7% PVA solution; then, 7.5% cross-linker solution was added in equal volume. Upon mixing, the boronate group cross-links PVA hydrogel, embedding the cell in the 3D gel matrix. The boronate group also cross-links the cis-diols of the cell surface glycans to PVA, thereby tethering the cell surface to the gel. We used the above gel made of 7.5% cross-linker (Gel 7.5%) for all the experiments in this study, except for one group in Fig. 1G, wherein we used a softer gel made of 5% cross-linker (Gel 5%). To rule out that the gel alone might affect Ca^{2+} signaling, we examined the Ca^{2+} signals in the in-gel cardiomyocytes at resting state; the data showed no spontaneous Ca^{2+} activity in resting cells before or after paced contraction (Fig. 2A). To examine whether individual gel component might affect cardiomyocytes, we preincubated rabbit ventricular myocytes with PVA or cross-linker alone, followed by perfusion with the normal Tyrode solution and

contraction measurement; neither PVA nor cross-linker treatment had any effect on contraction measured as fractional shortening (fig. S2).

Confocal imaging of Ca^{2+} signals

Confocal imaging of the Fluo-4 signals was primarily used to detect the Ca^{2+} sparks and waves, because Fluo-4 is among the most sensitive indicators for detecting small changes in the local Ca^{2+} signals owning to its high quantum yield. Cardiomyocytes were loaded with the Ca^{2+} indicator Fluo-4 and then embedded in the gel. Confocal imaging was performed with standard methods (47) with an Olympus FluoView FV1000 confocal microscope (inverted configuration) with a water immersion fluorescence objective UPlanSApo 60×, 1.2 numerical aperture (NA) (corrected for the thickness of the no. 1 glass coverslip that is used at the bottom of the perfusion chamber). Fluo-4 was excited with a 488-nm laser beam (laser power set to 5%), and the emitted fluorescence light was passed through a bandpass filter BA505-605 and collected with a photon multiplier tube (PMT). The PMT voltage, gain, and offset were set to avoid any saturation and to obtain high-fidelity images. The linescan images were obtained using the highest scan speed of 2 μs per pixel.

Ca^{2+} sparks were detected automatically using a custom program based on our spark identification algorithm and adapted for *x-t* linescan images (48). Sparks were identified in two stages. In the first stage, putative sparks are detected on the basis of Cheng *et al.*'s description (49), and bright but spatially small events were eliminated using our previously described “live-or-die” algorithm (50). In the second stage, the putative sparks were classified as sparks or noise on the basis of the statistical sieve as described in our previous publication (48). This analysis software provides automated and objective (agnostic through statistical sieving) detection and classification of the Ca^{2+} signaling events in confocal linescan images.

Fura-2 ratiometric measurement of Ca^{2+} concentration

To measure the intracellular Ca^{2+} concentration, we used Fura-2 dual-wavelength ratiometric method (46), which is more precise than using the Fluo-4 single-wavelength method. Isolated cardiomyocytes were continuously perfused in Tyrode solution containing 150 mM NaCl, 5.4 mM KCl, 1.2 mM $MgCl_2$, 1 mM $CaCl_2$, at pH 7.4, incubated with 2.5 μM Fura-2/acetoxymethyl (AM) and 0.75 μM Pluronic F127 (in 20% dimethyl sulfoxide) at room temperature for 30 min, washed embedded in the PVA gel, and used for experiments within 2 hours. Cells were paced at 0.5-Hz frequency by electrical field stimulation using short (4 ms) depolarization pulses with bipolar switching (switch positive and negative polarity in consecutive stimulus pulses) applied with a pair of platinum electrodes. Continuous perfusion of fresh Tyrode solution was used to maintain constant bath conditions (pH, glucose, ionic composition, temperature, and so on). An IonOptix system (IonOptix Inc.) with a HyperSwitch was mounted on the Olympus X71 inverted microscope with a water immersion fluorescence objective UPlanSApo 40×, 1.15 NA (corrected for the thickness of the no. 1 glass coverslip used as the bottom of the chamber). The excitation light was generated using a high-intensity arc lamp (Cairn). The galvanometer-based HyperSwitch delivered dual-excitation beams at 340 and 380 nm using a 340/370d/380 filter cube, switching between the two wavelengths at a frequency of 500 Hz. Fura-2 fluorescence

emission light was passed through a bandpass filter D510/40m and collected in a PMT. The background fluorescence signals at 340- and 380-nm channels were obtained in both the Tyrode solution and the gel without cells; the background signals were slightly higher in the gel than in the solution, but substantially lower than the Fura-2 fluorescence emissions from cells. The Fura-2 fluorescence ratio, R_{Fura}, was calculated from the fluorescence emissions from cells at 340- and 380-nm excitation wavelengths after background subtraction.

For measuring systolic Ca^{2+} transient, the cell was first paced to reach steady state (>2 min), and then Fura-2 fluorescence was recorded for at least 10 beats during steady state. For SR content measurement, after the cell reached steady state, field stimulation was stopped to keep the cell at a resting state for 15 s; then, caffeine at high concentration (20 mM) was applied to rapidly deplete the SR load. The rapidity of the SR Ca^{2+} release was accessed by the rising velocity of the caffeine-induced Ca^{2+} transient, and the peak Ca^{2+} value was used as an index to measure the SR load. As noted, the SR Ca^{2+} content measured using either Fura-2 (Fig. 2E) or Fluo-4 did not show any discernible difference between the cell-in-gel and the load-free contraction. Because RyR sensitivity to the intra-SR Ca^{2+} concentration is steep, we also acknowledge that small changes in SR Ca^{2+} content below the precision of the Fura-2 method could have a functional impact.

Structured illumination microscopy

We used a DeltaVision OMX V3.0 Blaze system (Applied Precision Inc.) to acquire the fluorescence images of antibody-labeled cardiomyocytes as previously described (51). Briefly, the system uses 488- and 532-nm lasers as the light source for illumination. A grating in the beam path generated three coherent beams that created 3D structured illumination patterns in the sample. The antibody-labeled cells were immersed in the ProLong Gold antifade reagent with 1.47 refractive index (RI), and fluorescence emission was collected with a 60× oil immersion objective with 1.514 RI, 1.42 NA. Fluorescence of different colors was separated by a dichroic mirror and filtered by bandpass emission filters before being collected by two fast sCMOS cameras (PCO-TECH Inc.). To acquire 3D images, the sample was moved along the *z* direction at a step size of 125 nm. For each slice, the illumination pattern was rotated three times and shifted five times, resulting in a total of 15 exposures per channel. Acquired raw images were processed with a proprietary software package (softWoRx v5.0, Applied Precision Inc.) to reconstruct super-resolution 3D images. Reconstructed images of different colors were registered using custom-built software to correct chromatic aberrations and image distortions. Before the experiments, the system and the color registration software were calibrated using multicolor polymeric beads of 0.1 μm (TetraSpeck beads, Molecular Probes). The spatial resolution of the system was ∼110 nm for the *x* and *y* axes and ∼250 nm for the *z* axis. The color registration error was smaller than a pixel (namely, 40 nm). 3D rendering of the SIM images was performed with Volocity Visualization package.

The colocalization of nNOS or eNOS with RyR was analyzed using Volocity Quantitation (PerkinElmer), implementing the standard Pearson's colocalization analysis (52). A user-defined threshold was set to separate signal from background, and Mander's overlapping coefficients (M1 and M2) were calculated (51). The extent of colocalization was measured

by M1and M2 values depicted by the overlapping regions (mixed color in the bars) in Fig. 3G. The bars represent the voxel volume of nNOS (green)–RyR (red) and eNOS (cyan)–RyR (red), each normalized to the RyR voxel volume. Note that M1 and M2 values give a general measure of colocalization, but do not quantify the physical distances between molecules.

The nearest-neighbor distance between NOS and RyR clusters was measured as the smallest pairwise distance between the center of mass of the respective molecular clusters (51). Objects (blobs) having a volume smaller than 0.00189 μm^3 (which might arise from photon noise) were excluded in the pairwise distance calculations. The center of mass and the nearest-neighbor distances were determined using the Volocity Quantitation software package.

Confocal imaging of antibody-labeled cells

Confocal images were obtained using an Olympus FluoView FV1000 confocal microscope (inverted configuration) with a water immersion fluorescence objective UPlanSApo 60×, 1.2 NA (corrected for the thickness of the no. 1 glass coverslip used at the bottom of the chamber). The water immersion objective was used to match the RI of the solution in which the cells are kept to minimize spherical aberration. The confocal aperture was set to 1 airy unit to obtain the thinnest optical sectioning for highest spatial resolution. The confocal images were acquired using 2D scan. For imaging dual labeled cells, the “sequential mode” was used to switch between the two excitation beams to minimize crosstalk between the spectra of the two different fluorophores. The emitted fluorescence lights were separated by dichroic mirror into two channels and passed through corresponding bandpass filters (BA505-525 for green and BA560-660 for red colors), and then collected with a PMT for each channel. The highest spatial resolution of the confocal images was ∼0.3 μm at the *x* and *y* axes, and 0.8 to 1 μm at the *z* axis.

Cardiomyocyte contraction measurement

We used the IonOptix sarcomere detection and fast Fourier transform (FFT) method rather than Fluo-4 confocal imaging edge detection to measure cardiomyocyte contraction because the latter may lose precision if the cell's ends move out of the focal plane during contraction. Contraction was measured using an IonOptix system (IonOptix Co.) with a high-speed camera (MyoCam-S, 240 to 1000 frames/s) to record sarcomere movement during cardiomyocyte contraction. The sarcomere pattern was then used to calculate the sarcomere length using an FFT algorithm. The fractional shortening was then calculated as the percentage of change in sarcomere length during contraction.

Statistical tests

The numerical values are calculated for the mean, SD, and SEM. Mean ± SEM values are shown in the bar charts in all figures. The number of cells in each experimental group was reported in the figure captions, and the cells in each group came from three to six individual animals. Given the biological variability among cells, each cell was treated as independent in the statistical tests, although multiple cells may come from one animal. For data with a normal distribution, Student's *t* test (unpaired unequal variance) was used to compare two

different groups. One-way ANOVA was used to compare multiple groups, and a Bonferroni posttest was used for pairwise comparisons. Two-way ANOVA was used to compare multiple groups with two distinct factors, with Bonferroni posttest for pairwise comparisons. For data with a nonnormal distribution, such as the nNOS-RyR and eNOS-RyR distance histograms in Fig. 3C, the Mann-Whitney test was used to compare between two groups. The difference was deemed significant if $P < 0.05$, and denoted $*P < 0.05$, $**P < 0.01$, and $***P < 0.001$. All statistical tests were performed with GraphPad Prism Software (http://www.graphpad.com/).

Supplementary Material

Refer to Web version on PubMed Central for supplementary material.

Acknowledgments

We thank W. J. Lederer (University of Maryland), R. Ross [University of California (UC), San Diego], and R. Moss (University of Wisconsin-Madison) for scientific discussions on mechanochemotransduction.

Funding: This work was funded by NIH R03-AG031944 to Y.C.-I., R01-HL90880 to L.T.I. and Y.C.-I., R21-HL108300 to K.S.L., R37-HL30077 to D.M.B., and R01-HL075274 and R01-HL085844 and VA Merit Review Grant I01 BX000576 to N.C. H.H. and R.S. were supported, in part, by T32-HL86350 Training Grant (to N.C.). T.Z. and J.C. were supported by the Center for Biophotonics Science and Technology, a designated National Science Foundation Science and Technology Center managed by UC Davis, under Cooperative Agreement No. PHY0120999. This work was also supported, in part, by the UC Proof of Concept Grant #247525 to K.S.L. and Y.C.-I, and the UC Davis Startup funds to Y.C.-I.

References and Notes

1. von Anrep G. On the part played by the suprarenals in the normal vascular reactions of the body. J Physiol. 1912; 45:307–317. [PubMed: 16993158]
2. Sarnoff SJ, Mitchell JH, Gilmore JP, Remensnyder JP. Homeometric autoregulation in the heart. Circ Res. 1960; 8:1077–1091. [PubMed: 13746560]
3. Nichols CG, Hanck DA, Jewell BR. The Anrep effect: An intrinsic myocardial mechanism. Can J Physiol Pharmacol. 1988; 66:924–929. [PubMed: 3214805]
4. Cingolani HE, Pérez NG, Cingolani OH, Ennis IL. The Anrep effect: 100 years later. Am J Physiol Heart Circ Physiol. 2013; 304:H175–H182. [PubMed: 23161880]
5. ter Keurs HE. Heart failure and Starling's law of the heart. Can J Cardiol. 1996; 12:1047–1057. [PubMed: 9191498]
6. Petroff MG, Kim SH, Pepe S, Dessy C, Marbán E, Balligand JL, Sollott SJ. Endogenous nitric oxide mechanisms mediate the stretch dependence of Ca^{2+} release in cardiomyocytes. Nat Cell Biol. 2001; 3:867–873. [PubMed: 11584267]
7. Prosser BL, Ward CW, Lederer WJ. Subcellular Ca^{2+} signaling in the heart: The role of ryanodine receptor sensitivity. J Gen Physiol. 2010; 136:135–142. [PubMed: 20660656]
8. Prosser BL, Ward CW, Lederer WJ. X-ROS signaling: Rapid mechano-chemo transduction in heart. Science. 2011; 333:1440–1445. [PubMed: 21903813]
9. Chirinos JA, Segers P. Noninvasive evaluation of left ventricular afterload: Part 2: Arterial pressure-flow and pressure-volume relations in humans. Hypertension. 2010; 56:563–570. [PubMed: 20733088]
10. Toischer K, Rokita AG, Unsöld B, Zhu W, Kararigas G, Sossalla S, Reuter SP, Becker A, Teucher N, Seidler T, Grebe C, Preub L, Gupta SN, Schmidt K, Lehnart SE, Krüger M, Linke WA, Backs J, Regitz-Zagrosek V, Schäfer K, Field LJ, Maier LS, Hasenfuss G. Differential cardiac remodeling in preload versus afterload. Circulation. 2010; 122:993–1003. [PubMed: 20733099]

11. Shin SH, Hung CL, Uno H, Hassanein AH, Verma A, Bourgoun M, Køber L, Ghali JK, Velazquez EJ, Califf RM, Pfeffer MA, Solomon SD. Valsartan in Acute Myocardial Infarction Trial (VALIANT) Investigators, Mechanical dyssynchrony after myocardial infarction in patients with left ventricular dysfunction, heart failure, or both. Circulation. 2010; 121:1096–1103. [PubMed: 20176989]
12. Onofiok, E.; Lam, KS.; Luo, J. Three dimensional cell adhesion matrix. Patent WO/2010/148346. 2010.
13. Grieve DJ, Byrne JA, Siva A, Layland J, Johar S, Cave AC, Shah AM. Involvement of the nicotinamide adenosine dinucleotide phosphate oxidase isoform Nox2 in cardiac contractile dysfunction occurring in response to pressure overload. J Am Coll Cardiol. 2006; 47:817–826. [PubMed: 16487851]
14. Shaw J, Izu L, Chen-Izu Y. Mechanical analysis of single myocyte contraction in a 3-D elastic matrix. PLOS One. 2013; 8:e75492. [PubMed: 24098388]
15. Stoyanovsky D, Murphy T, Anno PR, Kim YM, Salama G. Nitric oxide activates skeletal and cardiac ryanodine receptors. Cell Calcium. 1997; 21:19–29. [PubMed: 9056074]
16. Lim G, Venetucci L, Eisner DA, Casadei B. Does nitric oxide modulate cardiac ryanodine receptor function? Implications for excitation–contraction coupling. Cardiovasc Res. 2008; 77:256–264. [PubMed: 18006480]
17. Eisner DA, Choi HS, Díaz ME, O'Neill SC, Trafford AW. Integrative analysis of calcium cycling in cardiac muscle. Circ Res. 2000; 87:1087–1094. [PubMed: 11110764]
18. Barouch LA, Harrison RW, Skaf MW, Rosas GO, Cappola TP, Kobeissi ZA, Hobai IA, Lemmon CA, Burnett AL, O'Rourke B, Rodriguez ER, Huang PL, Lima JAC, Berkowitz DE, Hare JM. Nitric oxide regulates the heart by spatial confinement of nitric oxide synthase isoforms. Nature. 2002; 416:337–339. [PubMed: 11907582]
19. Feron O, Belhassen L, Kobzik L, Smith TW, Kelly RA, Michel T. Endothelial nitric oxide synthase targeting to caveolae. Specific interactions with caveolin isoforms in cardiac myocytes and endothelial cells. J Biol Chem. 1996; 271:22810–22814. [PubMed: 8798458]
20. Williams JC, Armesilla AL, Mohamed TMA, Hagarty CL, McIntyre FH, Schomburg S, Zaki AO, Oceandy D, Cartwright EJ, Buch MH, Emerson M, Neyses L. The sarcolemmal calcium pump, α-1 syntrophin, and neuronal nitric-oxide synthase are parts of a macromolecular protein complex. J Biol Chem. 2006; 281:23341–23348. [PubMed: 16735509]
21. Mohamed TMA, Oceandy D, Zi M, Prehar S, Alatwi N, Wang Y, Shaheen MA, Abou-Leisa R, Schelcher C, Hegab Z, Baudoin F, Emerson M, Mamas M, Di Benedetto G, Zaccolo M, Lei M, Cartwright EJ, Neyses L. Plasma membrane calcium pump (PMCA4)-neuronal nitric-oxide synthase complex regulates cardiac contractility through modulation of a compartmentalized cyclic nucleotide microdomain. J Biol Chem. 2011; 286:41520–41529. [PubMed: 21965681]
22. Burkard N, Rokita AG, Kaufmann SG, Hallhuber M, Wu R, Hu K, Hofmann U, Bonz A, Frantz S, Cartwright EJ, Neyses L, Maier LS, Maier SKG, Renné T, Schuh K, Ritter O. Conditional neuronal nitric oxide synthase overexpression impairs myocardial contractility. Circ Res. 2007; 100:e32–e44. [PubMed: 17272813]
23. Lai Y, Zhao J, Yue Y, Duan D. α2 and α3 helices of dystrophin R16 and R17 frame a microdomain in the α1 helix of dystrophin R17 for neuronal NOS binding. Proc Natl Acad Sci USA. 2013; 110:525–530. [PubMed: 23185009]
24. Szczesna D, Zhang R, Zhao J, Jones M, Guzman G, Potter JD. Altered regulation of cardiac muscle contraction by troponin T mutations that cause familial hypertrophic cardiomyopathy. J Biol Chem. 2000; 275:624–630. [PubMed: 10617660]
25. Chandra M, Rundell VL, Tardiff JC, Leinwand LA, de Tombe PP, Solaro RJ. Ca^{2+} activation of myofilaments from transgenic mouse hearts expressing R92Q mutant cardiac troponin T. Am J Physiol Heart Circ Physiol. 2001; 280:H705–H713. [PubMed: 11158969]
26. Yanaga F, Morimoto S, Ohtsuki I. Ca^{2+} sensitization and potentiation of the maximum level of myofibrillar ATPase activity caused by mutations of troponin T found in familial hypertrophic cardiomyopathy. J Biol Chem. 1999; 274:8806–8812. [PubMed: 10085122]

27. Morimoto S, Yanaga F, Minakami R, Ohtsuki I. Ca^{2+}-sensitizing effects of the mutations at Ile-79 and Arg-92 of troponin T in hypertrophic cardiomyopathy. Am J Physiol. 1998; 275:C200–C207. [PubMed: 9688851]
28. Watkins H, McKenna WJ, Thierfelder L, Suk HJ, Anan R, O'Donoghue A, Spirito P, Matsumori A, Moravec CS, Seidman JG, Seidman CE. Mutations in the genes for cardiac troponin T and α-tropomyosin in hypertrophic cardiomyopathy. N Engl J Med. 1995; 332:1058–1064. [PubMed: 7898523]
29. Hernandez OM, Housmans PR, Potter JD. Invited review: Pathophysiology of cardiac muscle contraction and relaxation as a result of alterations in thin filament regulation. J Appl Physiol. 2001; 90:1125–1136. [PubMed: 11181629]
30. Tardiff JC. Sarcomeric proteins and familial hypertrophic cardiomyopathy: Linking mutations in structural proteins to complex cardiovascular phenotypes. Heart Fail Rev. 2005; 10:237–248. [PubMed: 16416046]
31. Boyden PA, Barbhaiya C, Lee T, ter Keurs HE. Nonuniform Ca^{2+} transients in arrhythmogenic Purkinje cells that survive in the infarcted canine heart. Cardiovasc Res. 2003; 57:681–693. [PubMed: 12618230]
32. Berlin JR, Cannell MB, Lederer WJ. Cellular origins of the transient inward current in cardiac myocytes. Role of fluctuations and waves of elevated intracellular calcium. Circ Res. 1989; 65:115–126. [PubMed: 2736729]
33. Kass RS, Lederer WJ, Tsien RW, Weingart R. Role of calcium ions in transient inward currents and aftercontractions induced by strophanthidin in cardiac Purkinje fibres. J Physiol. 1978; 281:187–208. [PubMed: 702368]
34. Ferrier GR, Moe GK. Effect of calcium on acetylstrophanthidin-induced transient depolarizations in canine Purkinje tissue. Circ Res. 1973; 33:508–515. [PubMed: 4752852]
35. Girouard H, Wang G, Gallo EF, Anrather J, Zhou P, Pickel VM, Iadecola C. NMDA receptor activation increases free radical production through nitric oxide and NOX2. J Neurosci. 2009; 29:2545–2552. [PubMed: 19244529]
36. Guo T, Zhang T, Mestril R, Bers DM. Ca^{2+}/calmodulin-dependent protein kinase II phosphorylation of ryanodine receptor does affect calcium sparks in mouse ventricular myocytes. Circ Res. 2006; 99:398–406. [PubMed: 16840718]
37. Erickson JR, Patel R, Ferguson A, Bossuyt J, Bers DM. Fluorescence resonance energy transfer–based sensor Camui provides new insight into mechanisms of calcium/ calmodulin-dependent protein kinase II activation in intact cardiomyocytes. Circ Res. 2011; 109:729–738. [PubMed: 21835909]
38. Lou LL, Lloyd SJ, Schulman H. Activation of the multifunctional Ca^{2+}/calmodulin-dependent protein kinase by autophosphorylation: ATP modulates production of an autonomous enzyme. Proc Natl Acad Sci USA. 1986; 83:9497–9501. [PubMed: 3467320]
39. Erickson JR, Joiner MlA, Guan X, Kutschke W, Yang J, Oddis CV, Bartlett RK, Lowe JS, O'Donnell SE, Aykin-Burns N, Zimmerman MC, Zimmerman K, Ham AJL, Weiss RM, Spitz DR, Shea MA, Colbran RJ, Mohler PJ, Anderson ME. A dynamic pathway for calcium-independent activation of CaMKII by methionine oxidation. Cell. 2008; 133:462–474. [PubMed: 18455987]
40. Kentish JC, Wrzosek A. Changes in force and cytosolic Ca^{2+} concentration after length changes in isolated rat ventricular trabeculae. J Physiol. 1998; 506(Pt. 2):431–444. [PubMed: 9490870]
41. Alvarez BV, Pérez NG, Ennis IL, Camilión de Hurtado MC, Cingolani HE. Mechanisms underlying the increase in force and Ca^{2+} transient that follow stretch of cardiac muscle: A possible explanation of the Anrep effect. Circ Res. 1999; 85:716–722. [PubMed: 10521245]
42. Moolman JC, Corfield VA, Posen B, Ngumbela K, Seidman C, Brink PA, Watkins H. Sudden death due to troponin T mutations. J Am Coll Cardiol. 1997; 29:549–555. [PubMed: 9060892]
43. Maron BJ, Gardin JM, Flack JM, Gidding SS, Kurosaki TT, Bild DE. Prevalence of hypertrophic cardiomyopathy in a general population of young adults. Echocardiographic analysis of 4111 subjects in the CARDIA Study. Circulation. 1995; 92:785–789. [PubMed: 7641357]
44. Kockskämper J, von Lewinski D, Khafaga M, Elgner A, Grimm M, Eschenhagen T, Gottlieb PA, Sachs F, Pieske B. The slow force response to stretch in atrial and ventricular myocardium from

human heart: Functional relevance and subcellular mechanisms. Prog Biophys Mol Biol. 2008; 97:250–267. [PubMed: 18466959]

45. Seo K, Rainer PP, Lee DI, Hao S, Bedja D, Birnbaumer L, Cingolani OH, Kass DA. Hyperactive adverse mechanical-stress responses in dystrophic heart are coupled to TRPC6 and blocked by cGMP-PKG modulation. Circ Res. 2014; 114:823–832. [PubMed: 24449818]
46. Chen-Izu Y, Chen L, Bányász T, McCulle SL, Norton B, Scharf SM, Agarwal A, Patwardhan AR, Izu LT, Balke CW. Hypertension-induced remodeling of cardiac excitation-contraction coupling in ventricular myocytes occurs prior to hypertrophy development. Am J Physiol Heart Circ Physiol. 2007; 293:H3301–H3310. [PubMed: 17873027]
47. Kirk MM, Izu LT, Chen-Izu Y, McCulle SL, Wier WG, Balke CW, Shorofsky SR. Role of the transverse-axial tubule system in generating calcium sparks and calcium transients in rat atrial myocytes. J Physiol. 2003; 547:441–451. [PubMed: 12562899]
48. Bányász T, Chen-Izu Y, Balke CW, Izu L. A new approach to the detection and classification of Ca^{2+} sparks. Biophys J. 2007; 92:4458–4465. [PubMed: 17400702]
49. Cheng H, Song LS, Shirokova N, González A, Lakatta EG, Ríos E, Stern MD. Amplitude distribution of calcium sparks in confocal images: Theory and studies with an automatic detection method. Biophys J. 1999; 76:606–617. [PubMed: 9929467]
50. Chen-Izu Y, McCulle SL, Ward CW, Soeller C, Allen BM, Rabang C, Cannell MB, Balke CW, Izu LT. Three-dimensional distribution of ryanodine receptor clusters in cardiac myocytes. Biophys J. 2006; 91:1–13. [PubMed: 16603500]
51. Zhang T, Osborn S, Brandow C, Dwyre D, Green R, Lane S, Wachsmann-Hogiu S. Structured illumination-based super-resolution optical microscopy for hemato- and cytopathology applications. Anal Cell Pathol. 2013; 36:27–35.
52. Barlow AL, Macleod A, Noppen S, Sanderson J, Guérin CJ. Colocalization analysis in fluorescence micrographs: Verification of a more accurate calculation of Pearson's correlation coefficient. Microsc Microanal. 2010; 16:710–724. [PubMed: 20946701]

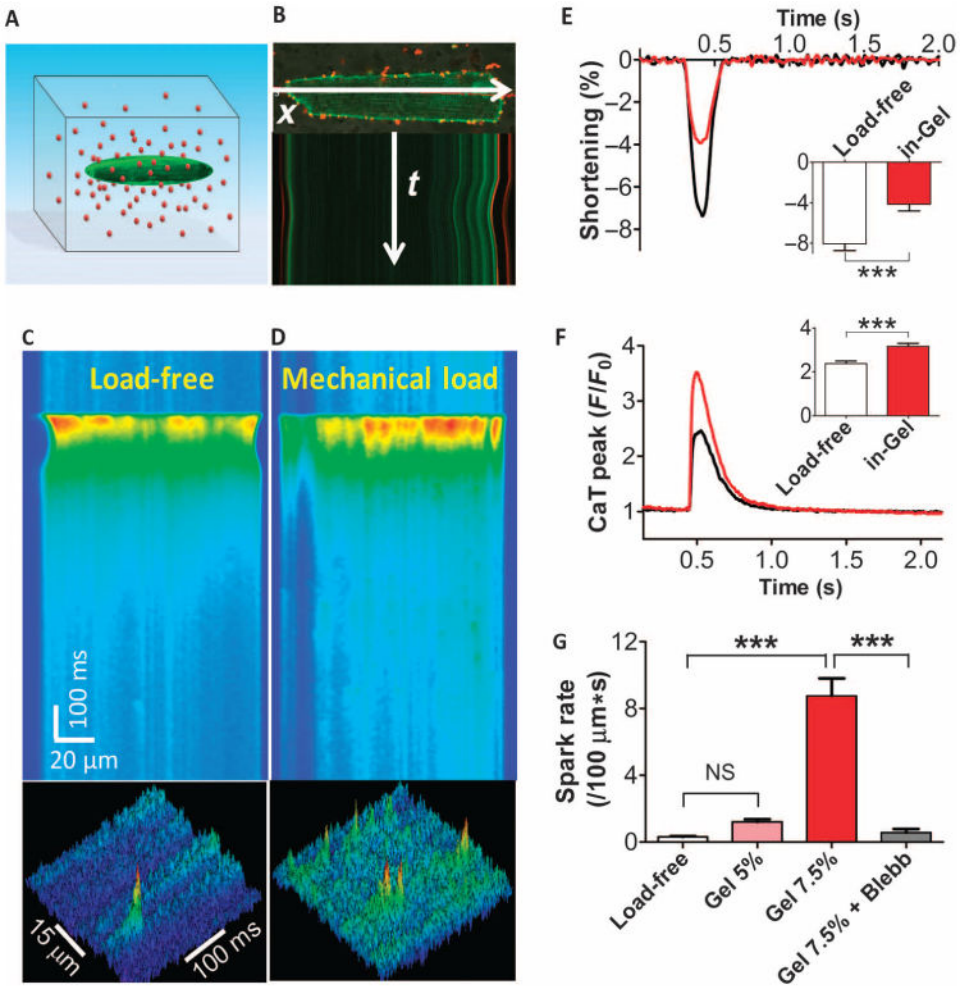

Fig. 1. The effects of mechanical stress on Ca^{2+} handling during systole and diastole

(**A**) Schematic of a cardiomyocyte embedded in 3D hydrogel matrix containing red fluorescence beads. (**B**) Confocal imaging of a cardiomyocyte and beads demonstrating cell contraction and gel deformation as seen in the movement of the cell's edge and the red fluorescent beads embedded in gel. (**C**) Cardiomyocytes contracting in normal Tyrode solution were designated the load-free control. Confocal linescan image shows the Ca^{2+} transient in bright fluorescence and the cell contraction in edge movement (upper panel); diastolic Ca^{2+} sparks are few (lower panel). (**D**) Cardiomyocytes contracting in-gel under mechanical load. The Ca^{2+} transient is high, and the cell contraction is small (upper panel); diastolic Ca^{2+} sparks are increased (lower panel). (**E**) Fractional shortening of cardiomyocyte contraction in-gel (n = 17 cells) compared with load-free control (n = 17). (**F**) Systolic Ca^{2+} transient (CaT) peak in cell-in-gel (n = 17) compared with load-free control (n = 17). (**G**) Diastolic Ca^{2+} spark frequency in cardiomyocytes that were load-free (n = 18) in soft gel made of 5% cross-linker (Gel 5%, n = 9), in gel with 7.5% cross-linker (Gel 7.5%, n = 18), and treated with blebbistatin (Blebb) (n = 5). One-way analysis of variance (ANOVA) with Bonferroni posttest was used for pairwise comparison; ***P < 0.001.

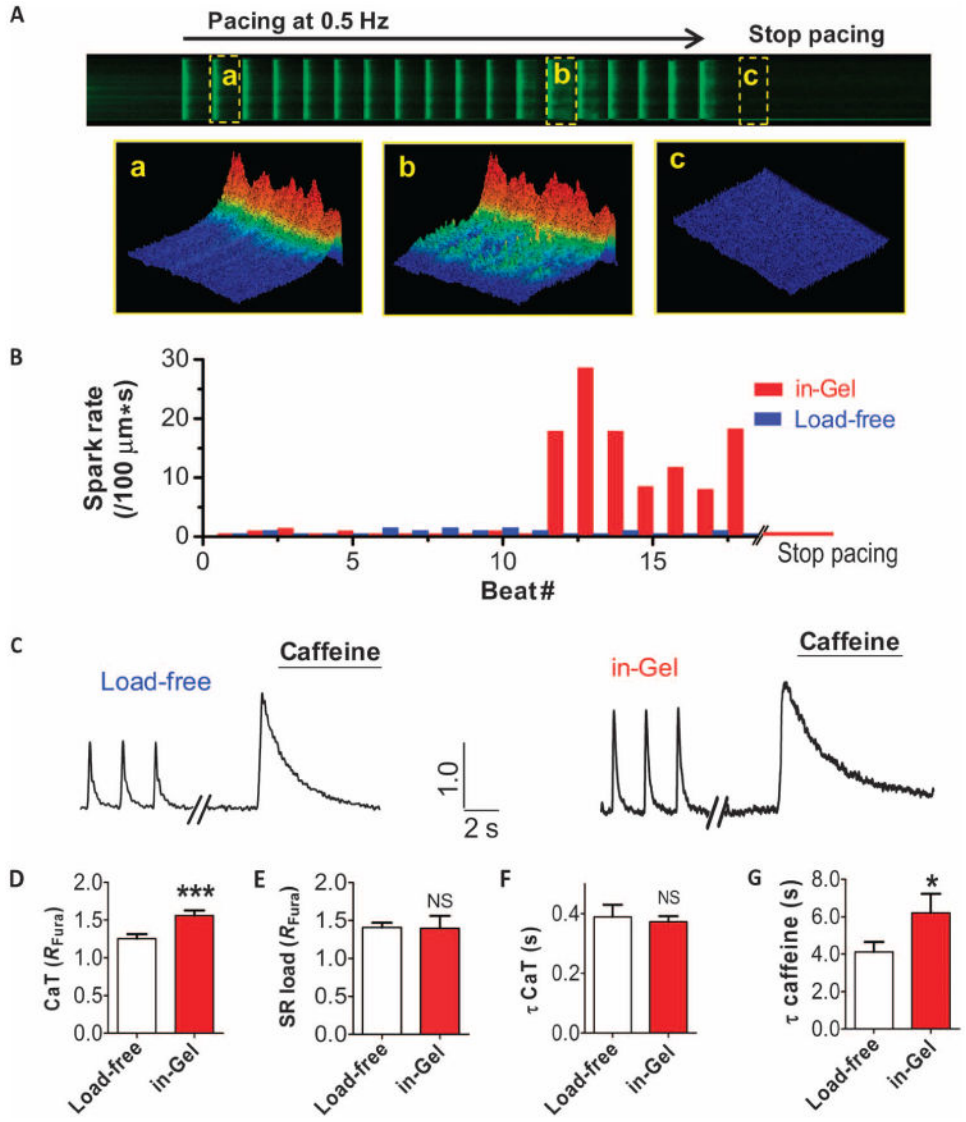

Fig. 2. Mechanochemotransduction and the SR load in contracting in-gel cardiomyocytes

Ca^{2+} signaling in cardiomyocytes was monitored before, during, and after pacing to assess the temporal response of mechanochemotransduction. (**A**) Representative cardiomyocyte in-gel had very few Ca^{2+} sparks before pacing; then, after an initial delay (a), it developed a large number of Ca^{2+} sparks during paced contraction (b); when pacing stopped, the Ca^{2+} sparks cleared out immediately (c). (**B**) Ca^{2+} spark rate in a representative cardiomyocyte contracting in-gel compared to a load-free cardiomyocyte during the pacing protocol. Similar data were obtained from 20 in-gel cells and 12 load-free cells. (**C**) Representative recordings of the Ca^{2+} transient (CaT) in a cardiomyocyte under load-free or in-gel contraction measured using Fura-2 ratio (R_{fura}). Scale bar: R = 0.5, t = 2 s. (**D**) The peak systolic Ca^{2+} transient is higher in-gel (n = 29 cells) than load-free (n = 19). (**E**) The SR content was measured by applying caffeine 15 s after pacing was stopped to rapidly release Ca^{2+} from SR. The SR content was similar for in-gel (n = 9) or load-free (n = 17) cardiomyocytes. NS, not significant. (**F**) τ of Ca^{2+} transient was not different for in-gel (n =

29 cells) or load-free (n = 19) cardiomyocytes. (**G**) τ of the caffeine-induced decrease in Ca^{2+} transient was higher for in-gel cardiomyocytes (n = 9) than for load-free cardiomyocytes (n = 17). Unpaired Student's t test; *P < 0.05, ***P < 0.001.

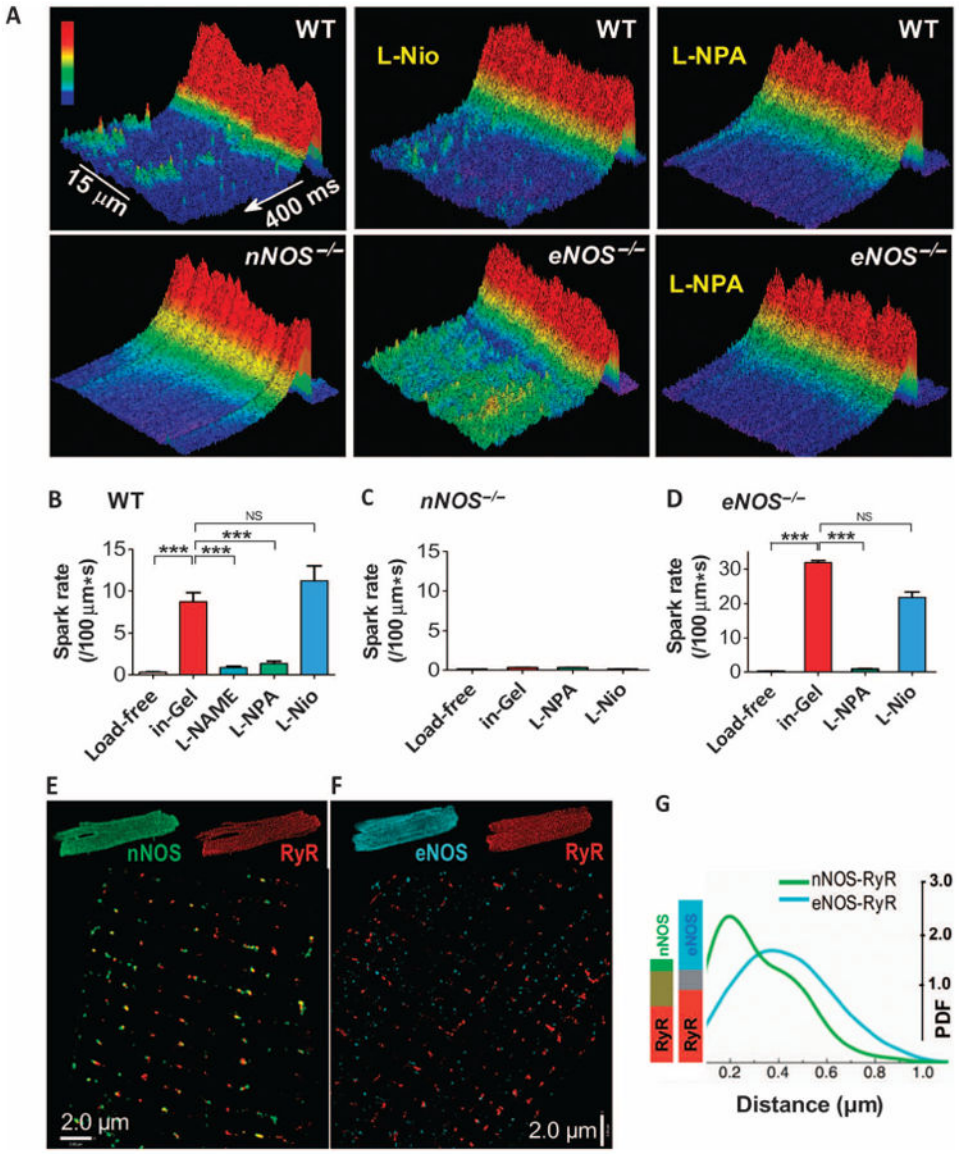

Fig. 3. Differential role for nNOS and eNOS in mechanochemotransduction

All data shown are from a cardiomyocyte contracting in-gel unless labeled Load-free. (**A**) The Ca^{2+} transient and spontaneous Ca^{2+} sparks seen in the 3D display of confocal linescan images of representative cardiomyocytes, obtained using Fluo-4 confocal imaging. (**B**) Mean ± SEM values of Ca^{2+} spark rate in wild-type (WT) cardiomyocytes under load-free conditions (n = 18 cells), in-gel (n = 18), and treated with L-NAME (n = 9), L-NPA (n = 9), or L-Nio (n = 10), respectively. (**C**) The Ca^{2+} spark rate in *nNOS*$^{-/-}$ cardiomyocytes: n = 8, 10, 10, and 9 cells for each group from left to right, respectively. (**D**) The Ca^{2+} spark rate in *eNOS*$^{-/-}$ cardiomyocytes: n = 10, 13, 6, and 6 cells for each group from left to right, respectively. One-way ANOVA with Bonferroni posttest was used for pairwise comparison; ***$P < 0.001$. (**E** and **F**) Representative SIM images of nNOS-RyR (E) and eNOS-RyR (F); n = 5 for each group. (**G**) Colocalization of nNOS-RyR and eNOS-RyR is depicted as the overlapping voxel volume (bars). Intermolecular distance histogram shows the probability

density function (PDF) of the nearest-neighbor distance (curves). The kink in the curve for nNOS-RyR distance indicates that there is more than one population for nNOS-RyR distances. The Mann-Whitney test was used to compare the nNOS-RyR and the eNOS-RyR distance histograms, and the difference was significant at $P < 0.0001$.

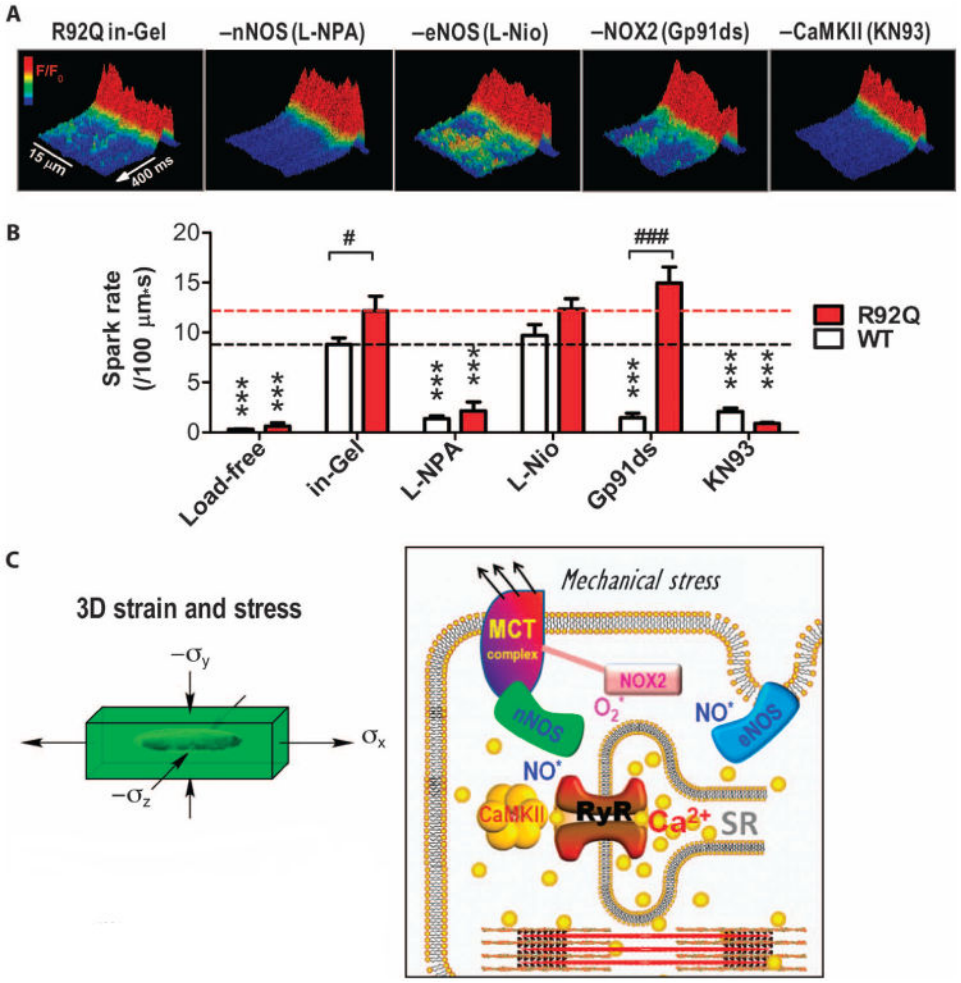

Fig. 4. Mechanochemotransduction in cardiomyocytes from healthy and cardiomyopathic hearts

(**A**) Sample images of Ca^{2+} signals in R92Q cardiomyocytes during pacing at 1 Hz at body temperature, and the effect of inhibiting NOS isoforms, NOX2, and CaMKII. (**B**) The Ca^{2+} spark rate in WT and R92Q cardiomyocytes. WT: load-free (n = 18 cells), cell-in-gel (n = 47), and cell-in-gel treated with L-NPA (n = 9), L-Nio (n = 9), Gp91ds (n = 31), or KN93 (n = 10). R92Q: load-free (n = 12), cell-in-gel (n = 20), and cell-in-gel treated with L-NPA (n = 32), L-Nio (n = 12), Gp91ds (n = 16), or KN93 (n = 23). Two-way ANOVA test shows significant difference in the spontaneous Ca^{2+} spark rate between the R92Q and WT ($P < 0.0001$), significant drug effects ($P < 0.0001$), and also significant interaction ($P < 0.0001$). Bonferroni posttest shows significant difference for the drug effect compared to cell-in-gel without drug (***$P < 0.001$) on each genotype; significantly higher spark rate in R92Q cardiomyocytes than in WT cardiomyocytes for cell-in-gel condition ($^{\#}P < 0.05$) and for Gp91ds effect ($^{\#\#\#}P < 0.001$) is also shown. (**C**) Schematic of the mechanochemotransduction pathway.